Holography with photoelectrons: a direct approach

2001 J. Phys.: Condens. Matter 13 10533

(http://iopscience.iop.org/0953-8984/13/47/302)

INSTITUTE OF PHYSICS PUBLISHING JOURNAL OF PHYSICS: CONDENSED MATTER

J. Phys.: Condens. Matter **13** (2001) 10533–10560 PII: S0953-8984(01)24639-6

Holography with photoelectrons: a direct approach

M Zharnikov[1] **and H-P Steinrück**[2]

[1] Angewandte Physikalische Chemie, Universität Heidelberg, Im Neuenheimer Feld 253, D-69120 Heidelberg, Germany
[2] Physikalische Chemie II, Universität Erlangen-Nürnberg, Egerlandstraße 3, D-91058 Erlangen, Germany

E-mail: Michael.Zharnikov@urz.uni-heidelberg.de

Received 8 May 2001, in final form 25 July 2001
Published 9 November 2001
Online at stacks.iop.org/JPhysCM/13/10533

Abstract

This article reviews the work performed by the authors regarding photoelectron holography on clean metal surfaces and simple adsorbate arrangements. The following systems were investigated: Pt(1 1 0)-1 × 2, Ni(1 1 0), Ni(1 1 1), Ni(1 1 0)-c(2 × 2) S, Ni(1 1 1)-p(2 × 2) S and Ni(1 1 1)-(5$\sqrt{3}$ × 2) S. The photoelectron diffraction patterns, which are interpreted as holograms, were recorded using synchrotron radiation at the German synchrotron facility BESSY-I in Berlin. For most systems these holograms were acquired at various kinetic energies. The real space structures were reconstructed from these data using the single wave number as well as the multiple wave number algorithm, without any prior assumptions. It was demonstrated that the local geometrical structure of clean single crystal surfaces and of adsorbate systems can be successfully reconstructed by using photoelectron holography with some restrictions.

1. Introduction

The determination of the adsorption geometry of molecules and molecular fragments on single crystal surfaces is central to many practical issues in surface science and, in particular, to our understanding of heterogeneous catalysis. The well-established techniques to determine the adsorbate structure such as low-energy electron diffraction and photoelectron diffraction suffer from the 'trial and error' nature of the approach and often rely on tremendous computational efforts. An alternative approach is photoelectron holography, which is a relatively new technique in surface science that has as yet to establish itself as a standard method to investigate the structures of surfaces. Its basic idea is that a photoelectron wave that is emitted from an internal source in the vicinity of a surface reaches the detector either directly or after scattering off neighbouring atoms, which can be considered as a reference and an object wave, respectively. Then, in analogy with conventional holography, the photoelectron diffraction

(PED) pattern $\chi(\boldsymbol{k})$, formed by coherent interference of the scattered and non-scattered photoelectron wavelets can be interpreted as a hologram [1, 2]. The three-dimensional image of the local structure around the emitter $U(\boldsymbol{r})$ can be numerically reconstructed from this hologram using a phased two-dimensional Fourier transformation [2]

$$U(\boldsymbol{r}) = \int \chi(\boldsymbol{k}) \mathrm{e}^{-\mathrm{i}\boldsymbol{k}\boldsymbol{r}} \, \mathrm{d}\boldsymbol{k}. \tag{1}$$

The theoretical spatial resolutions in the reconstructed image are different along the in-surface (Δx) and normal-to-surface (Δz) directions. In terms of the uncertainty principle they are determined by the absolute value of electron wave vector $\boldsymbol{k}$ and the collection semi-angle of the hologram $\theta_{\max}$ (the full opening angle is equal to $2\theta_{\max}$) [3, 4]

$$\Delta x \approx \pi/(k \times \sin\theta_{\max}) \qquad \Delta z \approx 2\pi/[k \times (1 - \cos\theta_{\max})]. \tag{2}$$

Considering the uncertainty principle once more, we can roughly estimate the maximum radius $r_{\max}$ at which meaningful information in real space may be obtained. This value is proportional to the inverse of the maximum uncertainty in the measurement of the electron momentum, i.e. to momentum Δk and angular $\Delta\theta$ resolutions [4]

$$r_{\max} \approx \pi/\Delta k = \pi/(k \times \Delta\theta). \tag{3}$$

Taking e.g. the Cu LMM Auger electrons with a kinetic energy of 914 eV ($k = 15.5$ Å^{-1}), $\theta_{\max} = 70^{\circ}$ and $\Delta\theta = 3^{\circ}$, one gets Δx, Δz and $r_{\max}$ equal to 0.2, 0.6 and 4.0 Å, respectively. Thus, at least the nearest neighbours of the emitter can be reconstructed with an atomic resolution.

However, for realistic atomic emitters and scatterers, the images of the atoms in the holographic reconstructions obtained from the PED patterns are distorted and displaced from the true positions. In addition to the atomic images, intense artefacts are observed, which cannot be distinguished from the true atomic images for systems with unknown crystallographic structure. The anisotropy of the electron reference wave, the strong anisotropy of the atomic scattering factor, multiple scattering events, self-interference and holographic twin images are believed to be the main sources of these phenomena. The strong forward-peaked nature of the atomic scattering factor in the relevant energy range (~300–1000 eV) is most disruptive in the so-called forward-scattering geometry, i.e. if the scatters are placed between the emitter and the detector [5, 6]. In the so-called back-scattering geometry, where the scatterers are further away from the detector than the emitter, the influence of this anisotropy on the PED pattern is somewhat weaker; nevertheless a combination of all other disruptive factors mentioned above can result in a deterioration of the holographic reconstruction [7].

Different strategies can be chosen to overcome the problems mentioned. Based on theoretical considerations, a correction for the anisotropy of the reference wave and the anisotropy of the atomic scattering factor can be included in the reconstruction algorithm [6–9], which leads in many cases to the correct reproduction of atomic positions [10, 11]. This procedure, however, requires an *a priori* knowledge of what must be corrected for and is also not compatible with the time-efficient fast Fourier transform code used in the usual reconstruction algorithm (equation (1)); it is therefore only applicable to limited space regions or along selected directions in real space. However, even within the usual reconstruction algorithm one can avoid problems associated with the strong anisotropy of the atomic scattering factor (especially in the forward-scattering geometry) by choosing an appropriate reference wave in the holographic experiment. It was shown theoretically that the disruptive zero-order diffraction fringes associated with forward scattering are noticeably suppressed for reference waves with high angular momentum character (f- and g-waves) [7].

A different approach to improving the quality of holographic reconstructions is to reinforce real single scattering contributions and to suppress multiple scattering, self-interference and twin image contributions by appropriate phase locking onto single scattering components. This can be achieved by an appropriate combination of photoelectron diffraction data measured at different kinetic energies of the outgoing electrons. For this purpose, the simple reconstruction algorithm (1) has been extended in different ways [12, 13]. One of them [12], which also includes a correction for the anisotropy of the atomic scattering factor, uses diffraction data taken in narrow angular cones centred around several supposed inter-atomic directions; this is well applicable for the forward-scattering geometry where these directions can be approximately determined from forward-focussing maxima (zero-order interference) in the diffraction pattern [14, 15]. In the back-scattering geometry, which is especially attractive for determining the structure of adsorbate systems, inter-atomic directions are, however, not marked by such pronounced structures. In this case one needs to carry out the calculations for expected back-scattering directions, which can lead to equivocal results because both the selection of the limited cones in the supposed back-scattering directions and the correction for the anisotropy of the electron-atom scattering are based on the assumption of the definite locations of the scattering atoms (see reference 12). The holographic reconstructions for different possible geometries must then be performed and compared with each other. This problem however, can be overcome when using a different multiple energy algorithm [13] where no assumptions about the surface geometry are necessary and multiple energy holograms collected over the full detection angle (preferably 2π) are used for the reconstruction. Initially, this so-called multiple wave number phased sum algorithm was only used for a limited number of objects in the forward-scattering geometry [15, 16], and its application for back-scattering geometry was demonstrated only for simulated data [13].

We have investigated the potential of photoelectron holography by applying it to simple systems, namely clean and adsorbate-covered metal surfaces. The following systems were studied: clean Ni(1 1 0) [17], Pt(1 1 0) [18, 19] and Ni(1 1 1) [19, 20], as well as c(2×2) S on Ni(1 1 0) [17] and p(2×2) S and ($5\sqrt{3} \times 2$) S on Ni(1 1 1) [19–21]. The clean metal surfaces (forward-scattering geometry) were chosen in such a way that the angular momentum character of the outgoing photoelectron wave was varied: the intense 3p (s/d wave) and 4f (d/g wave) photoemission signals were used for nickel and platinum surfaces, respectively. Thus, the theoretical considerations [7] concerning the suppression of the zero-order diffraction fringes by appropriate selection of the reference wave could be directly proven. The selected adsorbate superstructures were chosen due to their different complexity, which permits study of the power of photoelectron holography. These superstructures were investigated both in the forward- and back-scattering geometries using the photoemission signal from the substrate and adsorbate atoms, respectively.

One major goal of our work was to check the applicability of the multiple energy algorithm by Barton [13] to experimental data. For this purpose, the PED patterns (holograms) for all investigated systems, except for Ni(1 1 0) and Ni(1 1 0)-c(2×2) S, were measured at several kinetic energies and then processed (i) individually within the single energy approach [3] and (ii) together within the multiple wave number phased sum method [13]. This allows investigation of the possible energy dependence of the holographic reconstruction and comparison of the results obtained within these two approaches.

Another challenge was to find a way to reduce the very large experimental datasets usually associated with photoelectron holography (full-hemispherical PED patterns at various kinetic energies). For this purpose we checked the possibility of acquiring and processing the diffraction data in a defined angular sector only (at best in the symmetry-irreducible one) [19, 20].

In the following section the experimental procedure and data processing are addressed. Thereafter, experimental data for several clean and adsorbate-covered metal surfaces, which are used as test systems, are presented in section 3. On the basis of these data, different experimental and computational strategies for the practical 3D reconstruction of the adsorbate–substrate systems are discussed and practical recipes for the experiment, data processing and interpretation of the results are given. The results are summarized in section 4.

2. Experimental procedure and data processing

The experiments were performed in a two-chamber ultrahigh vacuum (UHV) system [22, 23] consisting of a preparation chamber and an analyser chamber. Details of crystal cleaning and the adsorbate superstructures preparation can be found everywhere [17–21]. All photoemission data were recorded at the synchrotron radiation facility BESSY I in Berlin using the HE-TGM 2 (High Energy Toroidal Grating Monochromator 2 [24]) at photon energies ranging from 295 to 490 eV and normal incidence.

The experiments for the clean surfaces were carried out at room temperature, whereas the measurements for the adsorbate superstructures were performed at temperatures of $\sim$100 K, which are particularly important for the back-scattering geometry to minimize the Debye–Waller losses and thereby to improve the contrast in the PED patterns [6]. Polar angle distributions were measured using a homebuilt toroidal angle multichannel electron energy analyser [25, 26] that allows the simultaneous detection of electrons emitted into a polar angle, θ, range from -10° to 90° for a fixed azimuth. The azimuthal angle was varied mechanically by rotating the sample around the surface normal, covering an azimuthal range of 126° in steps of 3°. Individual polar angle distributions were normalized with respect to the photon flux that was recorded independently during the measurements and were corrected for the corresponding background that was measured separately: $\chi(\boldsymbol{k}) = (I - I_0)/I_0$, where I and I_0 are the signal and background intensities, respectively. The full hemispherical angular distributions of the photoelectrons were then obtained by applying symmetry operations using the mirror planes of the crystal. For numerical processing, these distributions were projected onto square grids of 512×512 or 128×128 points in the (k_x, k_y) plane.

To isolate the holographic interference information $\chi'(\boldsymbol{k})$ from the raw electron angular distribution patterns $\chi(\boldsymbol{k})$ the low-frequency components of these patterns were suppressed by the Fourier filtering technique [4, 17]

$$\chi'(\boldsymbol{k}) = \chi(\boldsymbol{k}) - \chi(\boldsymbol{k}) \otimes G(\theta, \varphi) \tag{4}$$

where $G(\theta, \varphi)$ is a 2D Gaussian of defined angular width, which can be varied. This procedure allows part reduction in intense artefacts near the origin of the reconstructed images. As a first step, we have then carried out the holographic reconstruction using the single wave number approach equation (1) [2]. The amplitude of the reconstructed image $U(\boldsymbol{r})$ was calculated from the single-energy anisotropy function $\chi'(\boldsymbol{k})$ by

$$U(\boldsymbol{r}) = \int a(\boldsymbol{k})\chi'(\boldsymbol{k})\mathrm{e}^{-\mathrm{i}\boldsymbol{k}\boldsymbol{r}}\,\mathrm{d}\boldsymbol{k} \tag{5}$$

where $a(\boldsymbol{k}) = k_z/k$ is an apodizing function which is commonly used to minimize high-frequency aliasing effects caused by the finite range of integration over $\mathrm{d}\boldsymbol{k}$ [4]. The squared magnitude of $U(\boldsymbol{r})$ then represents the reconstructed three-dimensional image of the surface structure surrounding the emitter.

To obtain the amplitude of the reconstructed image $U(\boldsymbol{r})$ within the multiple wave number phased sum method, the data collected at different kinetic energies were processed together according to [13]

$$U(\boldsymbol{r}) = \sum U_k(\boldsymbol{r}) \times \mathrm{e}^{-\mathrm{i}\boldsymbol{kr}} \tag{6}$$

where $U_k(\boldsymbol{r})$ are the complex wave fields obtained from the anisotropy functions $\chi'(\boldsymbol{k})$ for each k separately according to equation (4) and $\exp(-\mathrm{i}\boldsymbol{kr})$ is the conjugate of the propagation phase shift for single scattering; it is exactly this factor that phase-locks the single scattering contribution of the individual reconstructed amplitudes.

Usually $\chi'(\boldsymbol{k})$ in equation (4) represents the anisotropy function in a cone centred around the surface normal, with a semi-angle that varies from 70 to 90° (in our case 90°). In optical holography it is, however, possible to reproduce a complete three-dimensional image not only from the complete hologram, but also from some individual part of it (albeit with lower resolution). As will be explained in more detail in section 3.1.1, due to the anisotropy of the atomic scattering factor for electrons, the information on the position of a specific atom in photoelectron holography is effectively localized in a certain region of the hologram: in forward-scattering geometry this region is a narrow cone in the forward-scattering direction [6, 27], and in the backscattering geometry it must also be some concentric region (broader than that for forward scattering) centred along scattering angles of 180° [5, 28]. To evaluate these effects we used not only full hemispherical angular PED patterns for the holographic reconstruction, but also those over the azimuthal sector of measurements (126°). In this case the angular distributions of the photoelectrons over the remaining azimuthal sector of 234° were first obtained using symmetry operations and then cut away again after Fourier filtering and multiplication by the apodizing function; this procedure prevents the appearance of strong spikes (in the **k** space) at the edges (step functions in the **k** space) of the experimental azimuthal sector that appear when Fourier filtering has been applied directly to it; note that no symmetry operations have been applied to the data in the sector used for reconstruction. For better visualization, the intensities obtained by the holographic reconstructions were transformed to a binary format. An eight-bit gray scale was used (except for the case of Ni(1 1 0)-c(2 × 2) S).

3. Results and Discussion

3.1. Clean metal surfaces

3.1.1. Ni(1 1 0). Nickel has fcc bulk structure. The schematic drawing of the Ni(1 1 0) surface is depicted in figure 1. The constants of the surface unit cell are 2.49 and 3.52 Å along the [1 $\underline{1}$ 0] and [0 0 1] directions respectively; the distance of successive (1 1 0) planes in the bulk (parallel to the surface) is 1.245 Å. For the top two surface layers a relaxation of 3–9% was reported (see discussion in reference 17).

For this surface we have measured only one single-energy PED pattern, namely the angular distribution of the Ni $3p_{3/2}$ photoelectrons with a kinetic energy of 273.2 eV. This pattern [17] is dominated by forward-scattering maxima, which show that the anisotropy of the atomic scattering factor is still pronounced, even at the relatively low kinetic energy. The anisotropy, the forward-scattering geometry and the unfavourable s/d character of the outgoing photoelectron wave resulted in rather poor quality of the holographic reconstruction, as is evident from figure 2, where (a) represents a cut in a plane parallel to the surface at $z =$ 1.245 Å (the first plane above the emitter), (b) a cut in a vertical plane parallel to the ($\underline{1}$ 1 0) plane at $x = 1.25$ Å, and (c) a cut in a vertical plane parallel to the (0 0 1) plane at $y = 1.76$ Å.

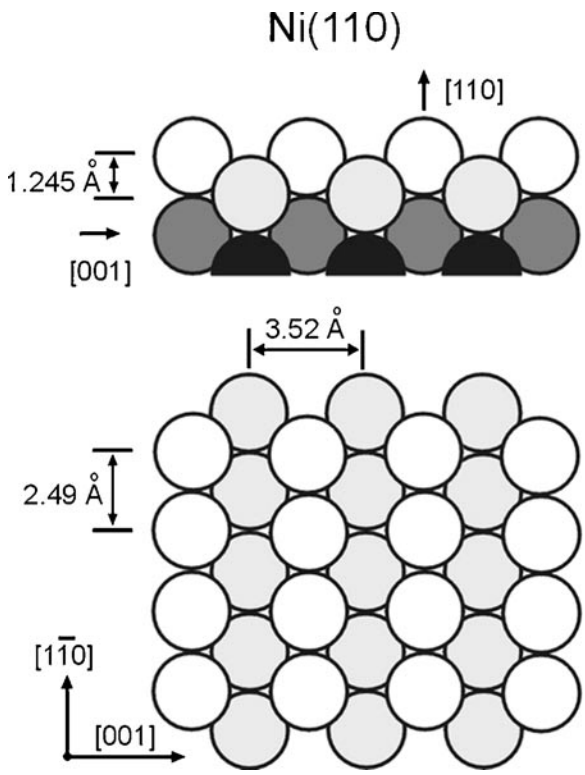

Figure 1. Side and top views of Ni(1 1 0).

In addition to the features at or near the expected locations of atoms (marked by the crosses), numerous intense artefacts are observed (see also other reconstructions in reference 17); an unequivocal determination of the atomic positions is thus not possible. The only satisfactory reconstruction was obtained in the plane of the emitter, parallel to the surface ($z = 0$). The maxima in the corresponding reconstruction (figure 3) show good agreement with the correct atomic positions of an ideal Ni(1 1 0) substrate and allow the identification of atoms up to the fourth coordinate sphere, which is related to the rather low k value and the relatively good angular resolution in our experiment: $r_{max} = 14.1$ Å (see equation (3)). The maxima in the reconstructed image show deviations from the correct positions of the order of an expected resolution of 0.4 Å. Also, the widths of the maxima compare well with this value.

The exceptionally good quality of the reconstruction at $z = 0$ is attributed to the suppression of the most distorted diffraction fringes for the atoms in this particular plane. Let us consider that the intensities and the positions of diffraction fringes in the realistic PED pattern differ from those in the analogous pattern for an idealized isotropic atomic scatterer. In the latter case, diffraction fringes due to an individual scatterer represent a system of concentric circles (whose periodicity depends on the wave vector value k and the distance between the emitter and scatterer r) in the emitter–scatterer direction [6]. In reality, the strong anisotropic character of the scattering factor results in a rapid decay of the intensity of the diffraction fringes with an increasing scattering angle, so that only the diffraction fringes close to the emitter–scatterer axis have sufficient intensity to contribute to the measurable holographic information. This means that the information about a particular atom is not spread over the complete diffraction

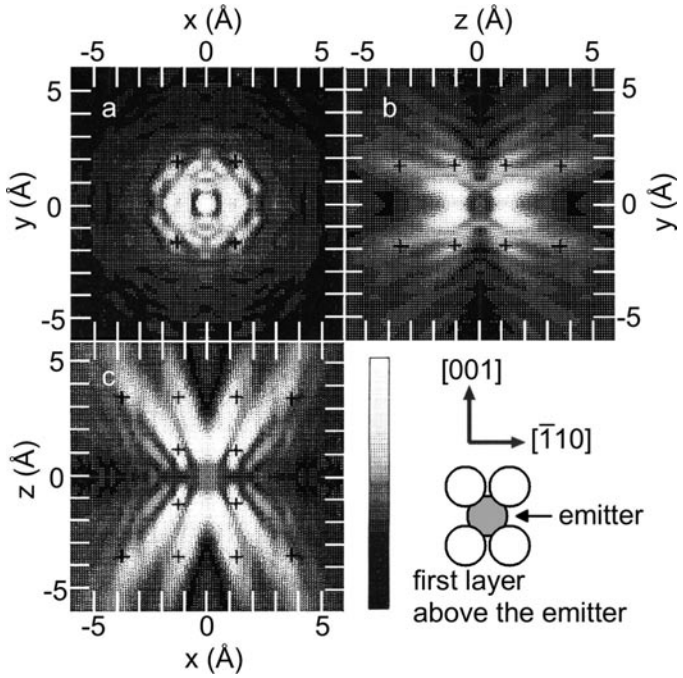

Figure 2. Holographic reconstruction of the Ni(1 1 0) crystal. (a) represents a cut in a plane parallel to the surface at $z = 1.245$ Å (the first plane above the emitter), (b) a cut in a vertical plane parallel to the ($\underline{1}$ 1 0) plane at $x = 1.25$ Å, and (c) a cut in a vertical plane parallel to the (0 0 1) plane at $y = 1.76$ Å. The crosses mark the expected locations of the Ni atoms. The shown directions and the schematic drawing of the crystallographic structure are related to a cut (a).

pattern, but is effectively concentrated in a narrow cone in a forward-scattering direction. At the same time, the angular variation of the phase of the scattering factor affects the periodicity of the diffraction structure [7] which leads to a displacement and broadening of the reconstructed atomic images. This distortion is, however, most pronounced for the first several diffraction fringes in the emitter–scatterer direction. These distorted fringes are effectively suppressed for the $z = 0$ plane because the emitter–scatterer direction corresponds to a take-off angle of 90°. The lower part of the diffraction cone is directed towards the crystal and is not acquired, whereas the upper part of this cone is suppressed by the apodizing function (see equation (5)) in such a way that the fringes which are closest to the emitter–scatterer direction are most attenuated. Thus the holographic information on the atom locations in the $z = 0$ plane is effectively provided by the almost undistorted diffraction fringes corresponding to the medium scattering angles, which seem to be intense enough to dominate over the noise in the PED pattern. Note, however, that in spite of all these considerations, the quality of the holographic reconstructions for Ni(1 1 0) should depend on the kinetic energy, as will be shown in the next section.

3.1.2. Ni(1 1 1). A schematic drawing of the Ni(1 1 1) surface is depicted in figure 4. This surface is characterized by P3M1 symmetry. The constant of surface reference cell is 2.49 Å and the distance of the successive (1 1 1) planes (normal to the surface) is 2.03 Å. A small top layer contraction of 0.025 ± 0.025 Å has been proposed [29, 30].

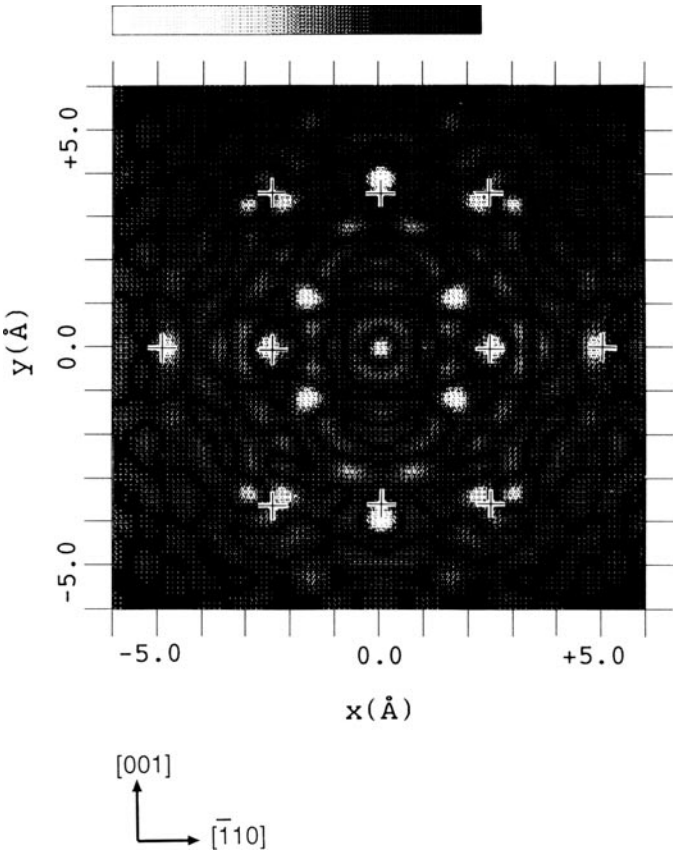

Figure 3. Holographic reconstruction of the Ni(1 1 0) crystal in the plane of emitter parallel to the surface from the Ni $3p_{3/2}$ PED hologram acquired at a kinetic energy of 273.2 eV. The crosses mark the expected locations of the atoms in the (1 1 0) plane of a Ni crystal.

For Ni(111) we have measured angular distributions of the Ni $3p_{3/2}$ photoelectrons ($E_B = 65.7$ eV) at seven different kinetic energies ranging from 239 eV ($k = 7.92$ Å^{-1}) to 417 eV ($k = 10.46$ Å^{-1}). The primary goal was to test both the single (at different kinetic energies) and the multiple wave number approaches in the forward-scattering geometry. The positions of the most intense maxima in the Ni $3p_{3/2}$ PED patterns [20] correlate within 2–3° with the [1 0 1], [1 1 2], [0 0 1], [1 0 2], [0 1 2] and symmetry-equivalent directions, as is expected for forward scattering. Only for the lowest kinetic energies some of these maxima become diffuse indicating a decrease in the forward-scattering character of the atomic scattering factor.

The real space structure was reconstructed using both the single (equation (5)) and the multiple (equation (6)) wave number algorithms. Although the latter approach resulted in an improvement of the reconstruction quality, the general results were the same as for clean Ni(1 1 0). Except for the reconstruction at $z = 0$, lots of very intense artefacts were observed together with the features at or near the expected locations of atoms [20]. The reconstructions at $z = 0$ are depicted in figure 5; the centre of the circles mark the true positions of the nickel atoms. The quality of the reconstructions depend on the kinetic energy: only for four energies, namely 268.8, 298.7, 328.2 and 357.5 eV are the atomic images of the six nearest neighbours the dominating structure in the emitter plane (note that for Ni(1 1 0) a kinetic energy of 273.3 eV, which is close to 268.8 eV, also led to a successful reconstruction); for

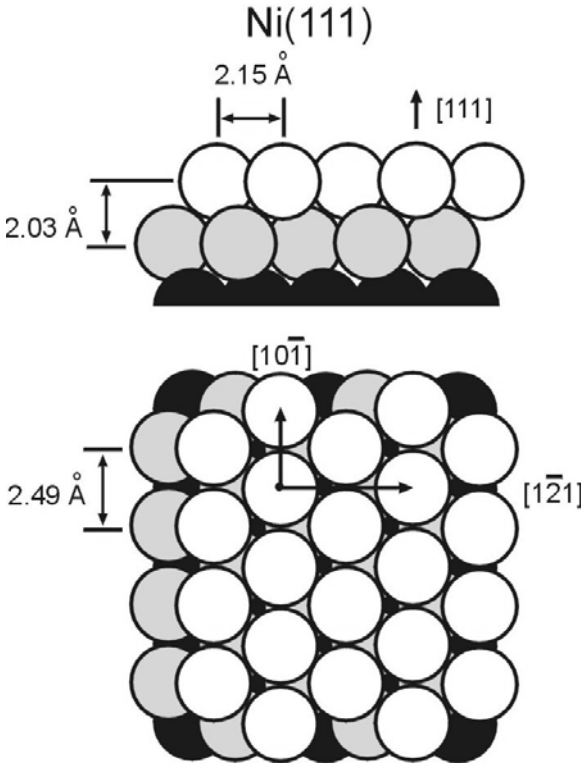

Figure 4. Side and top views of Ni(1 1 1).

328.2 eV even the six next nearest neighbours are observed. However, for 239 and 417.1 eV, holographic reconstructions in the emitter plane represent a mixture of atomic images and artefacts and for 387.3 eV the latter completely dominate. The dependence of magnitude and phase of the atomic scattering factor on kinetic energy seems to be essential for the holographic fringes, which are responsible for the atomic spots in the respective reconstructions. Thus, even at $z = 0$, the selection of a particular kinetic energy does not guarantee good quality of the reconstruction. This quality can however, be, significantly improved if the holograms acquired at different kinetic energies are processed together within the multiple wave number reconstruction approach (equation (6)). In fact, the expected positions of Ni atoms are well reproduced in the corresponding reconstruction in figure 5, although some artefacts are still not completely suppressed. One should note that a similar dependence of the quality of the reconstruction on the kinetic energy is to be expected for Ni(1 1 0) (see previous section). The concentration of the holographic information in a narrow cone centred in the forward-scattering direction permits the reconstruction of particular scatterers using only this part of the 2π PED pattern. In figure 6 holographic reconstructions of the Ni(1 1 1) surface in the $z = 0$ plane obtained from the Ni $3p_{3/2}$ 268.8 eV hologram using equation (5) and from seven different Ni $3p_{3/2}$ holograms using the multiple wave number reconstruction approach (equation (6)) are shown. Only diffraction data within the sector of measurements (126°, shown in the schematic drawing below) were used. Evidently, only the two Ni atoms having intense diffraction fringes inside this sector are well reproduced in figure 6(b). In figure 6(a)

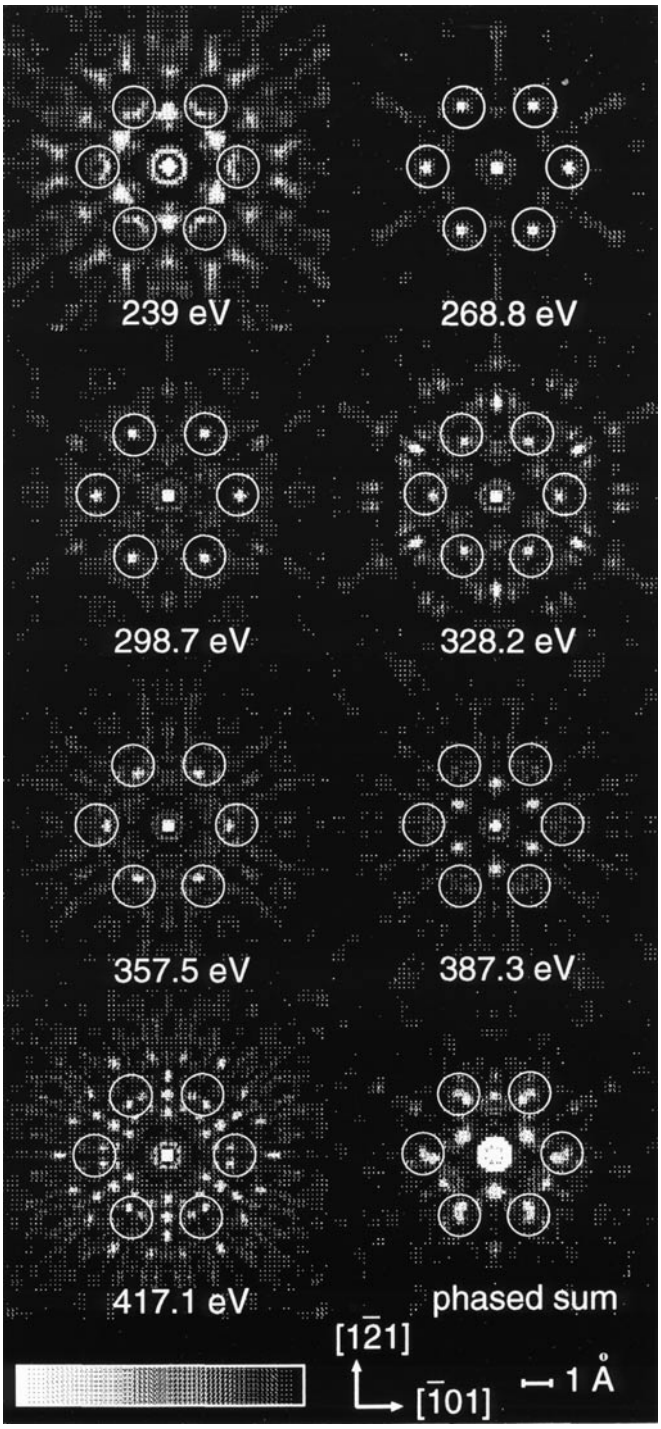

Figure 5. Holographic reconstructions in the emitter plane parallel to the surface ($z = 0$), obtained for the Ni(1 1 1) surface from individual Ni $3p_{3/2}$ holograms using equation (5) and from seven different Ni $3p_{3/2}$ holograms using the multiple wave number reconstruction approach (equation (6)). The centres of the circles mark the correct positions of the Ni atoms.

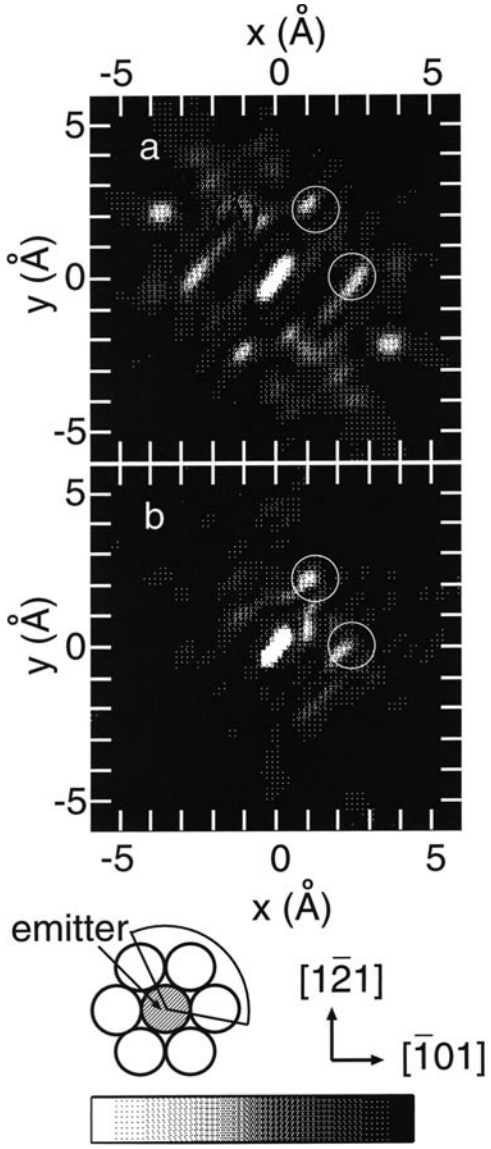

Figure 6. Holographic reconstructions in the $z = 0$ plane obtained for the Ni(1 1 1) surface from (a) the Ni $3p_{3/2}$ PED hologram at $E_{kin} = 268.8$ eV and (b) from seven different Ni $3p_{3/2}$ PED holograms using the single (equation (5)) and multiple (equation (6)) wave number reconstruction approach, respectively. Only diffraction data within the sector of measurements (126°, shown in the schematic drawing below) were used. The centres of the circles mark the correct positions of the Ni atoms lying inside the sector.

the real atomic spots are accompanied by the corresponding twin images, which are eliminated within the multiple wave number reconstruction approach due to appropriate phase locking.

3.1.3. Pt(1 1 0). The clean Pt(1 1 0) surface exhibits a 'missing row' reconstruction with every second row along the [1 $\underline{1}$ 0] direction missing, as depicted in figure 7. The constants

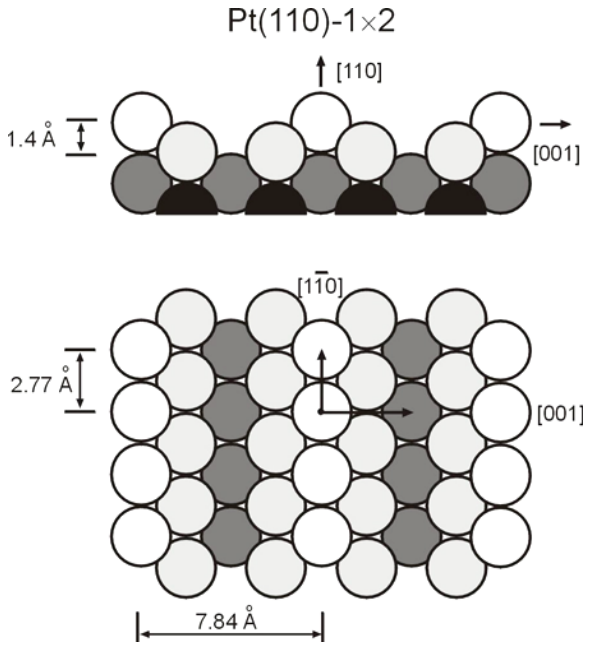

Figure 7. Side and top views of Pt(1 1 0).

of the surface reference cell of the Pt(110)-1 × 2 surface are 2.77 and 7.84 Å. The interlayer spacing normal to the surface is about 1.4 Å.

We have measured PED patterns of Pt $4f_{7/2}$ ($E_B = 71.2$ eV) and Pt $4f_{5/2}$ ($E_B = 74.5$ eV) photoelectrons at six kinetic energies ranging from 120 eV ($k = 5.61$ Å^{-1}) to 370 eV ($k = 9.85$ Å^{-1}). The primary goal was to suppress the disruptive effects related to the forward-scattering character of the electron-atom scattering factor by the selection of the photoelectron wave with a high angular momentum (d/g wave) and a relatively small kinetic energy. Overall, the results obtained from the both photoemission lines are very similar. For most kinetic energies the photoelectron intensities of both the $4f_{7/2}$ and $4f_{5/2}$ lines are predominantly concentrated in the (0 0 1), (1 1 1) and symmetry equivalent planes [18]. Forward-scattering maxima are also observed, but are rather diffuse. As for the Ni(1 1 1) surface, the quality of the reconstructed images (positions of atoms, intensity of artefacts) obtained using the single wave number algorithm strongly depends on the kinetic energy of the photoelectrons. This is illustrated in figure 8 where holographic reconstructions of the Pt(1 1 0)-1 × 2 surface obtained from the Pt $4f_{7/2}$ holograms at (A) 222.4 eV and (B) 369.3 eV using the single wave number algorithm as well as that obtained from all six Pt $4f_{7/2}$ holograms acquired at different kinetic energies using the multiple wave number method (C) are depicted. In each case (a) represents a cut in a plane parallel to the surface at $z = 1.4$ Å (the first plane above the emitter) and (b) shows a cut in a vertical plane parallel to the (0 0 1) plane at $y = 1.96$ Å. For 369.3 eV (figure 8(B)) the images are dominated by maxima attributed to the nearest neighbours in the plane above the emitter (the centres of the circles mark the correct positions of these atoms); for 222.4 eV (figure 8(A)) numerous intense artefacts are seen. The spots observed at the correct atomic positions in the first successive plane below the emitter (at $z = -1.4$ Å, see the vertical cuts in figures 8(A) and (B)) do not stem from the diffraction fringes related to the atoms in this plane, but represent the twin image of the atoms in the plane above the emitter.

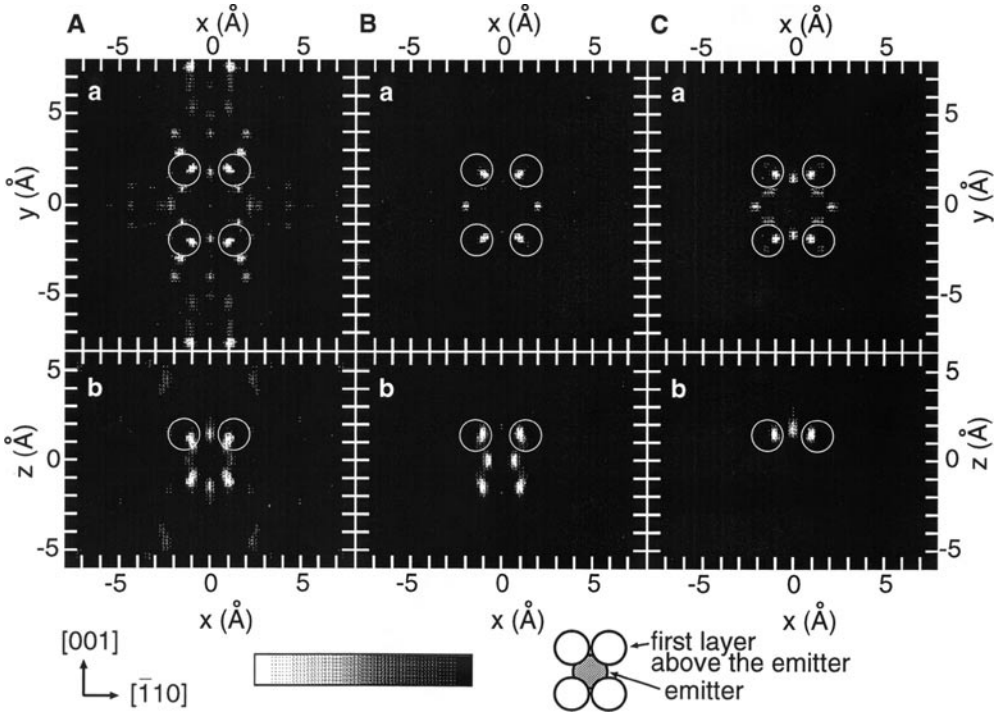

Figure 8. Holographic reconstructions of clean Pt(1 1 0)-1 × 2, obtained from Pt $4f_{7/2}$ PED holograms at (A) $E_{kin} = 222.4$ eV and (B) $E_{kin} = 369.3$ eV using the single wave number algorithm (equation (5)) and (C) from six different Pt $4f_{7/2}$ PED holograms using the multiple wave number algorithm. For all reconstructions (a) represents a cut in a plane parallel to the surface at $z = 1.4$ Å (the first plane above the emitter) and (b) a cut in a vertical plane parallel to the (0 0 1) plane at $y = 1.96$ Å. The centres of the circles mark the expected positions of the Pt atoms. The shown directions and the schematic drawing of the crystallographic structure are related to cuts (a).

Because of the anisotropy of the atomic scattering factor the strong diffraction fringes within the forward-scattering cones dominate over the weak back-scattering fringes.

The multiple wave number approach (figure 8(C)) leads to a strong suppression of the twin image at $z = -1.4$ Å, a reduction of certain artefacts and some improvement in lateral resolution. Although the atomic images are shifted from their true values by 0.2–0.3 Å, the obtained, almost artefact-free construction allows the unequivocal identification of the atomic environment in the vicinity of the emitter.

Furthermore, the atoms in the emitter plane parallel to the surface ($z = 0$) can be reconstructed in the same manner as for Ni(1 1 0) and Ni(1 1 1). The general quality of the holographic reconstructions is, however, somewhat worse than that for Ni(1 1 0) and Ni(1 1 1) (at $z = 0$) except for the reconstructions obtained from the holograms acquired at the lowest kinetic energies. The latter reconstructions are especially interesting because they can be associated with the 1 × 2 reconstructed topmost layer of Pt(1 1 0) due to the very small electron escape length at kinetic energies of ∼100 eV. Generally, the emitter can be located in every layer in the vicinity of the surface, but the signal from the deeper layers is strongly attenuated at small kinetic energies. In figure 9 holographic reconstructions of clean Pt(1 1 0)-1 × 2 obtained from the Pt $4f_{7/2}$ PED holograms at (A) $E_{kin} = 122.7$ eV and (B) $E_{kin} = 119.3$ eV using the single wave number algorithm (equation (5)) are presented. For both

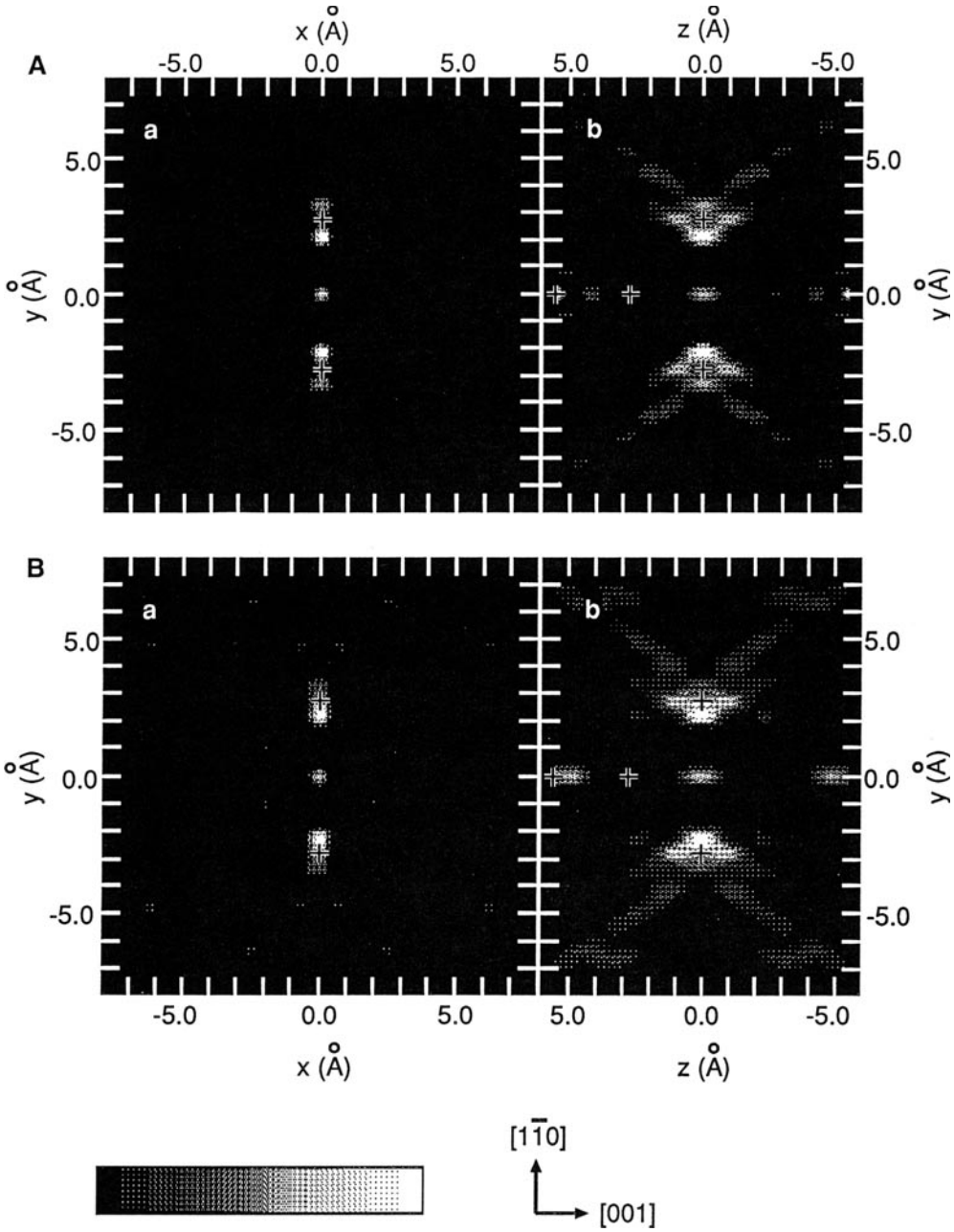

Figure 9. Holographic reconstructions of clean Pt(1 1 0)-1 × 2, obtained from Pt $4f_{7/2}$ PED holograms at (A) $E_{kin} = 122.7$ eV and (B) $E_{kin} = 119.3$ eV using the single wave number algorithm (equation (5)). For both reconstructions (a) represents a cut in a plane parallel to the surface at $z = 0$ Å and (b) a cut in a vertical plane parallel to the (0 0 1) plane at $x = 0$ Å. The crosses mark the expected positions of the Pt atoms. The shown directions are related to cuts (a).

reconstructions (a) represents a cut in a plane parallel to the surface at $z = 0$ Å and (b) a cut in a vertical plane parallel to the (0 0 1) plane at $x = 0$ Å. The nearest emitter neighbours along

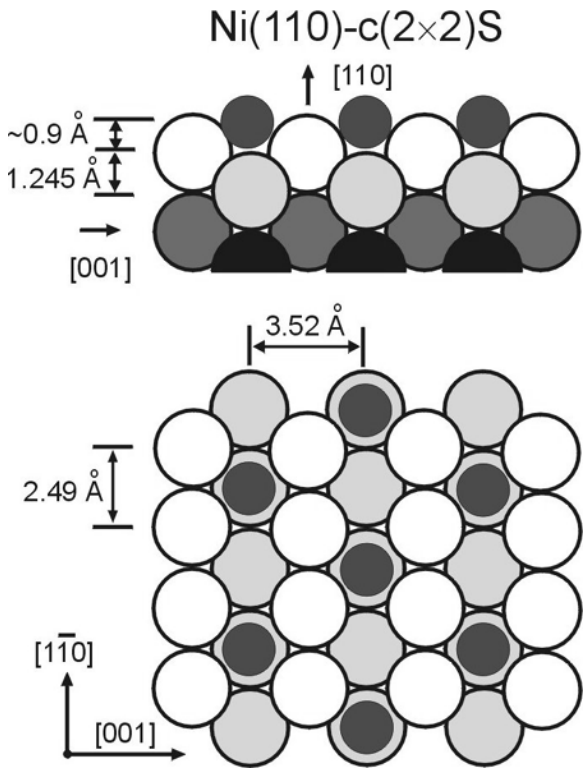

Figure 10. Side and top view of Ni(1 1 0)-c(2 × 2) S.

the [1 1 0] direction (i.e. along the densely packed rows) can be clearly identified. The images of these atoms dominate over all other features. Considering that the nearest neighbours along the [0 0 1] direction for the unreconstructed surface are placed at a distance of 3.92 Å (which is comparable with 2.77 Å along the [1 $\underline{1}$ 0] direction) and are absolutely not observed in the horizontal cuts in figure 9, we believe that these cuts clearly prove the 1×2 reconstruction of the Pt(1 1 0) surface. For the reconstructed surface, the next neighbours along the [0 0 1] direction are 7.84 Å away from the emitter and, thus, too far to be reconstructed (they are beyond the region in real space where meaningful information can be obtained).

A comparison of the results for Pt(1 1 0) with those for Ni(1 1 0) and Ni(1 1 1) clearly shows the importance of the choice of a proper reference wave in the forward-scattering geometry. While the reconstruction at $z = 0$ is a special case (see the comments in section 3.1.1), a successful reconstruction of the atoms above the emitter is only possible if the most intense forward-scattering artefacts are suppressed.

3.2. Adsorbate systems

3.2.1. Ni(1 1 0)-c(2 × 2) S. A schematic drawing of the Ni(1 1 0)-c(2 × 2) S system is presented in figure 10. The sulfur atoms are believed to be adsorbed in fourfold-coordinated hollow sites at a distance from the topmost Ni plane of ∼0.9 Å [31–33].

For this system we have measured the PED patterns of Ni $3p_{3/2}$, S $2p_{1/2}$ and S $2p_{3/2}$ photoelectrons at kinetic energies of 273.2 eV ($k = 8.47$ Å^{-1}), 178.2 eV ($k = 6.86$ Å^{-1}) and 179.2 eV ($k = 6.84$ Å^{-1}), respectively. Our goal was to reconstruct the structure of

the adsorbate system using the photoelectron lines of both the adsorbate and substrate atoms. Comparison of the Ni $3p_{3/2}$ PED pattern with the corresponding hologram of the clean Ni(1 1 0) surface shows that no significant changes occur on S adsorption [17]. Also, the holographic reconstructions from the former pattern practically do not differ from those obtained for the clean Ni(1 1 0). No additional features that could be attributed to the adsorbate atoms were observed in the reconstructed images [17]. There are two different reasons for this fact. First, the atomic number of S (14) and, consequently, the cross section of electron scattering that is responsible for the intensity of the object wave are relatively small. Second, the position of the c(2 × 2)S superstructure is different relative to the various planes of Ni, which contain the sources of the reference wave (non-equivalent emitters). Thus, it is almost impossible to reconstruct an adsorbate superstructure using a photoelectron line of the substrate, unless the atomic number of the adsorbate is noticeably larger than that of the substrate atoms.

The problem of non-equivalent emitters is, however, circumvented when using the sulfur atoms as sources of the reference waves, because all emitters are located in the same plane and have the same atomic environment (i.e. a definite adsorption site). Due to the larger atomic number of Ni and a shorter distance to the nearest Ni neighbours below the emitter than to the nearest S neighbours in the adsorbate plane, it should be much easier to reconstruct the former neighbours as compared to the latter. In fact, the holographic reconstructions in the adsorbate plane are dominated by very strong artefacts and only weak spots are found at the expected positions of the S atoms [17]. As to the nearest Ni neighbours, the corresponding holographic reconstructions obtained from the S $2p_{1/2}$ PED hologram at $E_{kin} = 178.2$ eV (A) and S $2p_{3/2}$ PED hologram at $E_{kin} = 179.2$ eV (B) using the single wave number algorithm (equation (5)) are presented in figure 11. For both reconstructions (a) represents a cut in a plane parallel to the surface at $z = -0.9$ Å (the surface of the substrate), (b) represents a cut in a vertical plane parallel to the (1 1 0) plane at $x = 1.25$ Å, and (c) represents a cut in a vertical plane parallel to the (0 0 1) plane at $y = 1.76$ Å. The crosses mark the expected positions of the Ni atoms for the case of a substrate–adsorbate distance of 0.9 Å and a fourfold-coordinated hollow adsorption site. The holographic reconstructions in figure 11 reproduce the expected atomic positions of the Ni atoms in the topmost layer fairly well. The deviations of the atomic spots from the correct positions and the widths of these spots in figure 11 are of the order of the expected spatial resolution. However, the reconstructions still exhibit intense artefacts that can impede an unequivocal identification of the 'real' atomic spots for unknown systems. Thus, whereas the electron holography approach seems to work for back-scattering geometry, the problem of the artefacts has to be overcome. Considering that in this geometry the artefacts are predominantly related to multiple scattering, self-interference and twin image contributions, the multiple wave number algorithm, which suppresses these contributions, has to be tried.

3.2.2. Ni(1 1 1)-p(2 × 2) S. The adsorbate system Ni(111)-p(2 × 2) S has been investigated before by various methods, including LEED [31, 34], SEXAFS [35] and low-energy ion scattering [36, 37]. The adsorption site was identified as the threefold fcc hollow site (data in reference 35 were not good enough to distinguish between the hcp and fcc hollow sites) with the distance from the top nickel plane varying between 1.4 and 1.7 Å. A schematic drawing of the Ni(1 1 1)-p(2 × 2) S system is presented in figure 12.

For this system we have measured angular distributions of S $2p_{3/2}$ photoelectrons ($E_B =$ 162 eV) for seven different kinetic energies ranging from 130 eV ($k = 5.84$ Å^{-1}) to 322.5 eV ($k = 9.2$ Å^{-1}). These relatively low kinetic energies have been chosen to increase the back-scattering cross section. The obtained PED patterns reveal a strong dependence on the kinetic energy of the photoelectrons, which is due to the energy dependence of the atomic scattering

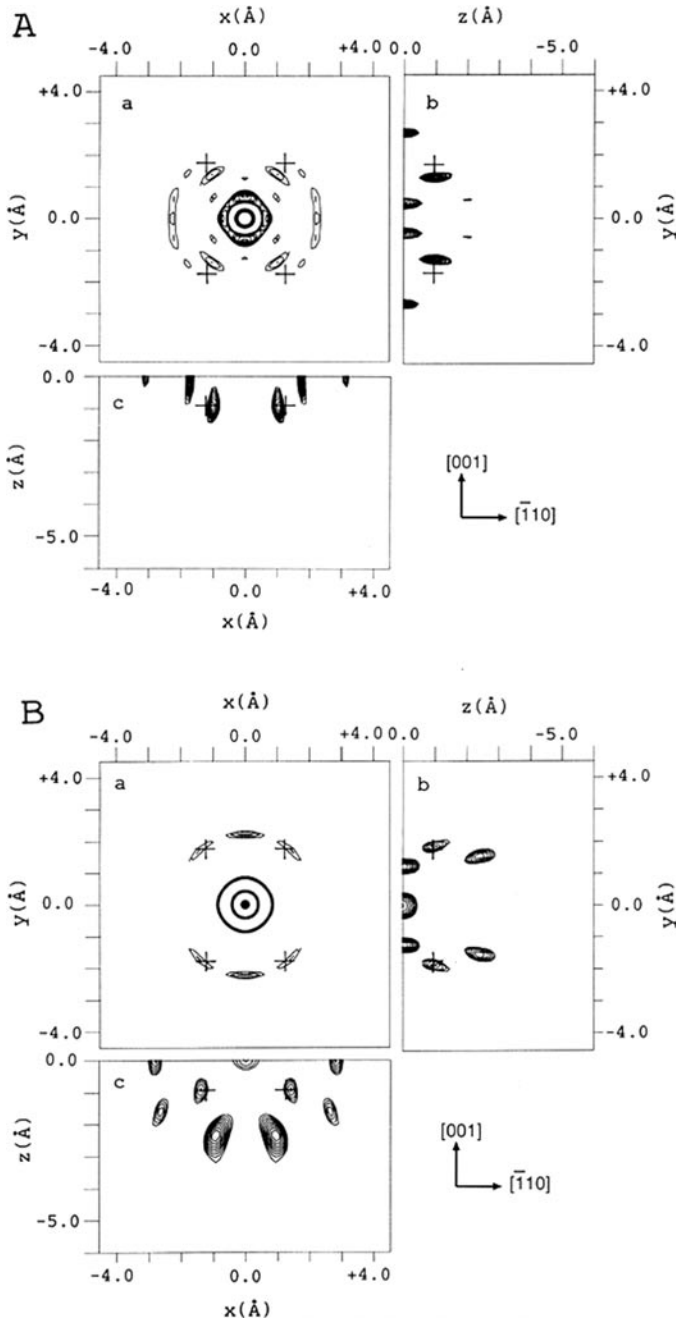

Figure 11. Holographic reconstructions of Ni(1 1 0)-c(2 × 2) S, obtained from the S $2p_{1/2}$ PED hologram at $E_{kin} = 178.2$ eV (A) and S $2p_{3/2}$ PED hologram at $E_{kin} = 179.2$ eV (B) using the single wave number algorithm (equation (5)). For both reconstructions (a) represents a cut in a plane parallel to the surface at $z = -0.9$ Å (the surface of the substrate), (b) a cut in a vertical plane parallel to the (1 1 0) plane at $x = 1.25$ Å, and (c) a cut in a vertical plane parallel to the (0 0 1) plane at $y = 1.76$ Å. The crosses mark the expected positions of the Ni atoms for the case of a substrate–adsorbate distance of 0.9 Å and a fourfold-coordinated hollow adsorption site. The shown directions are related to cuts (a).

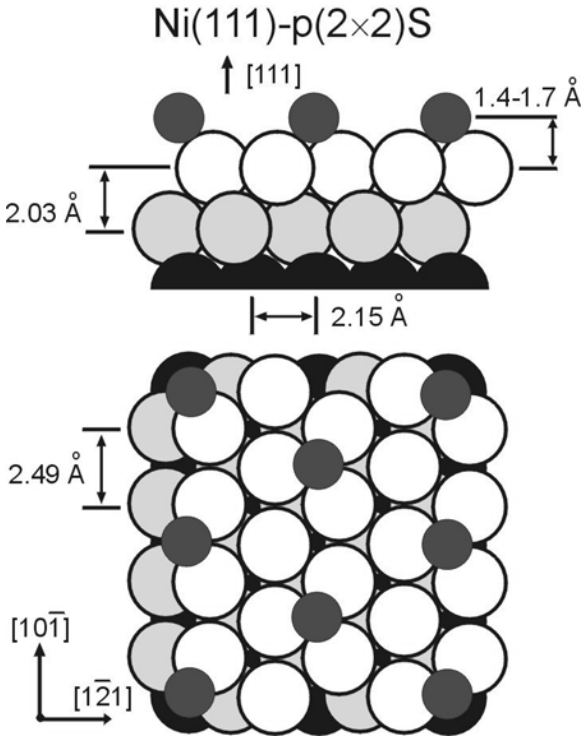

Figure 12. Side and top view of p(2 × 2)S/Ni(1 1 1).

factor [20, 21]. The results of the single wave number holographic reconstruction are, in general, similar to those for Ni(1 1 0)-c(2 × 2) S: whereas the atomic images in the emitter plane have only weak intensity as compared to the numerous artefacts, Ni atoms below the emitter can be reconstructed, even if the individual reconstructions show a dependence on the kinetic energy. The single wave number reconstructions from the individual S $2p_{3/2}$ holograms in the plane $z = -1.6$ Å (the topmost Ni layer) are depicted in figure 13 along with the multiple wave number reconstruction. For low kinetic energies (130 and 174.5 eV) no pronounced structures except a strong artificial feature directly below the emitter have been observed. For higher kinetic energies, the atomic images (albeit split and shifted for 204.5 and 293 eV) of the three nearest Ni atoms of an S fcc adsorption site are clearly visible. The atomic images for 233.5 and 322.5 eV have a lower intensity than the artefacts. Only for a kinetic energy of 263.5 eV does the intensity of the atomic images exceed that of the artefacts and atomic images not only of the nearest, but also of the next nearest Ni atoms are observed. For this energy, cuts in three mutually perpendicular planes passing through the atomic images of the nearest Ni neighbours are depicted in figure 14: cut (a) corresponds to a plane parallel to the surface at $z = -1.6$ Å (below the emitter, the same plane as in figure 13); cuts (b) and (c) represent planes perpendicular to the surface along the [1 $\underline{2}$ 1] and [$\underline{1}$ 0 1] directions. The centres of the circles mark the expected positions of the nickel atoms according to the fcc adsorption site of S. The symmetrical character of the holographic reconstruction with respect to the origin due to the superposition of real and twin images is clearly observed in figure 14(b) where the twin image of one of the Ni atoms is clearly visible in the $z = 1.6$ Å plane.

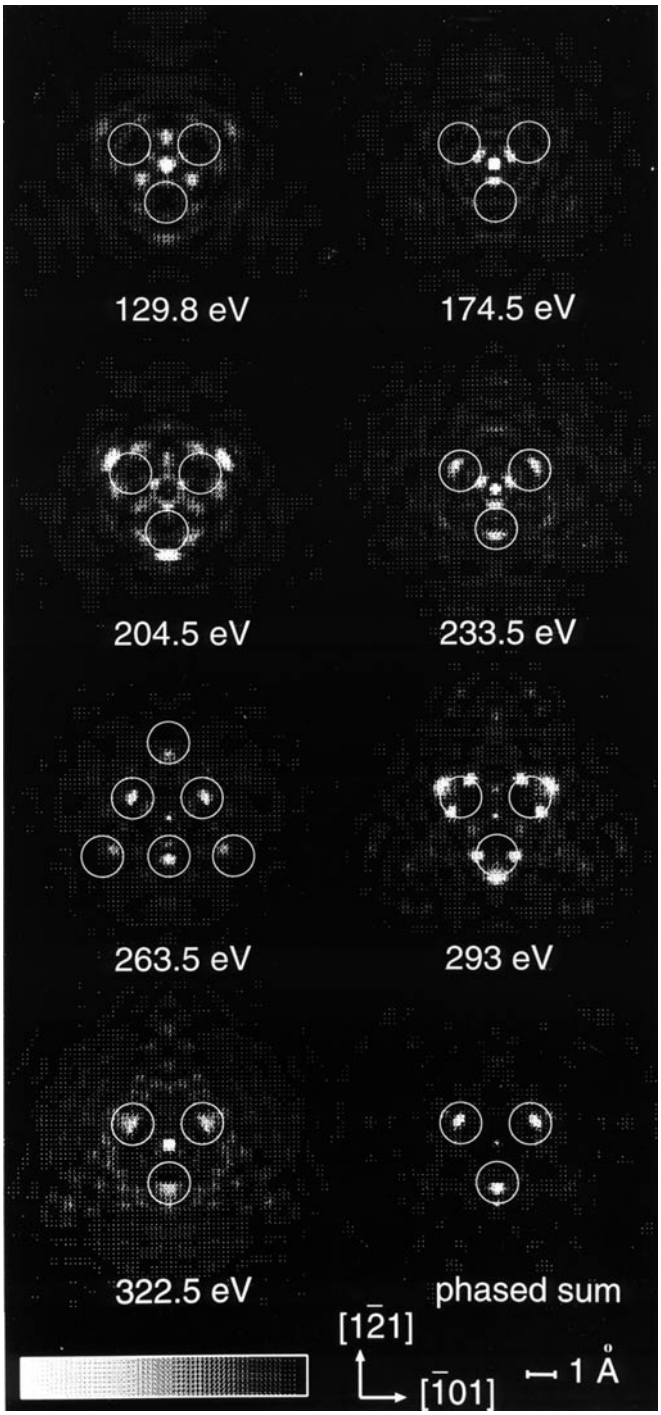

Figure 13. Holographic reconstructions in the plane parallel to the Ni(1 1 1) surface at $z = -1.6$ Å (the surface of the substrate), obtained for the p(2 × 2)S/Ni(1 1 1) structure from individual S $2p_{3/2}$ holograms and from seven different S $2p_{3/2}$ holograms using the single and multiple wave number reconstruction approaches, respectively. The centres of the circles mark the expected positions of the Ni atoms for the case of a substrate–adsorbate distance of 1.6 Å and the fcc adsorption site.

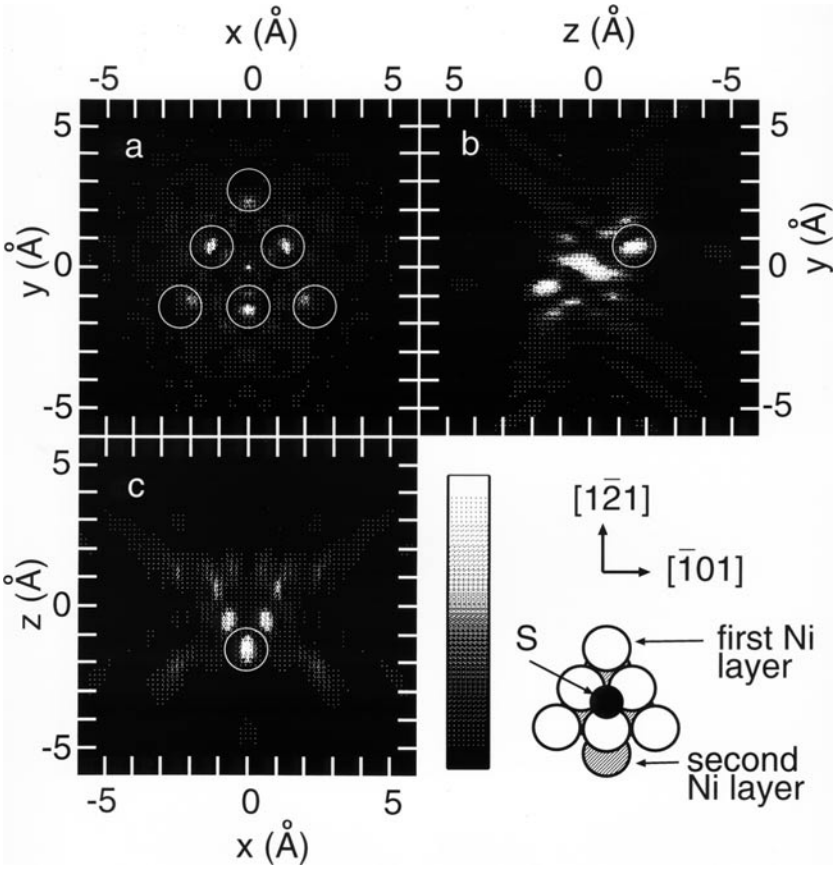

Figure 14. Holographic reconstruction obtained for the p(2 × 2)S/Ni(111) structure from the S $2p_{3/2}$ hologram at 263.5 eV using the single wave number reconstruction approach (equation (5)). (a) represents a cut in the plane parallel to the Ni(1 1 1) surface at $z = -1.6$ Å (the surface of the substrate), (b) cut in a vertical plane parallel to the ($\underline{1}$0 1) plane at $x = 1.43$ Å, and (c) cut in a vertical plane parallel to the (1 $\underline{2}$ 1) plane at $y = 1.59$ Å. Note that cuts (b) and (c) are shifted from the 'correct' positions at $x = 1.25$ Å and $y = 1.44$ Å, respectively, to pass through the atom images. The centres of the circles mark the expected positions of the Ni atoms for the case of a substrate–adsorbate distance of 1.6 Å and the fcc adsorption site. The directions shown and the schematic drawing of the crystallographic structure are related to cut (a).

Despite good agreement of some single wave number reconstructions for $z < 0$ with the fcc adsorption site of S on Ni(1 1 1), the identification is not straightforward due to the observed differences of individual single wave number reconstructions in this region. This problem is overcome by the multiple wave number phased sum approach (equation (6)), as seen from figure 13 (bottom, right) and figure 15, where the same cuts as in figure 14 (but obtained within the multiple wave number reconstruction method) are presented. The atomic images of three nearest neighbours in the plane $z = -1.6$ Å are clearly visible in the cuts and completely dominate in the physically meaningful region ($z < 0$) of the reconstruction (except strong artificial features near the origin). These images allow the unequivocal determination of the adsorption site of S on Ni(1 1 1) as a threefold fcc hollow site in complete agreement with the results of previous investigations. The adsorbate substrate distance can be clearly determined to ∼1.6 Å from the cuts normal to the plane of emitter.

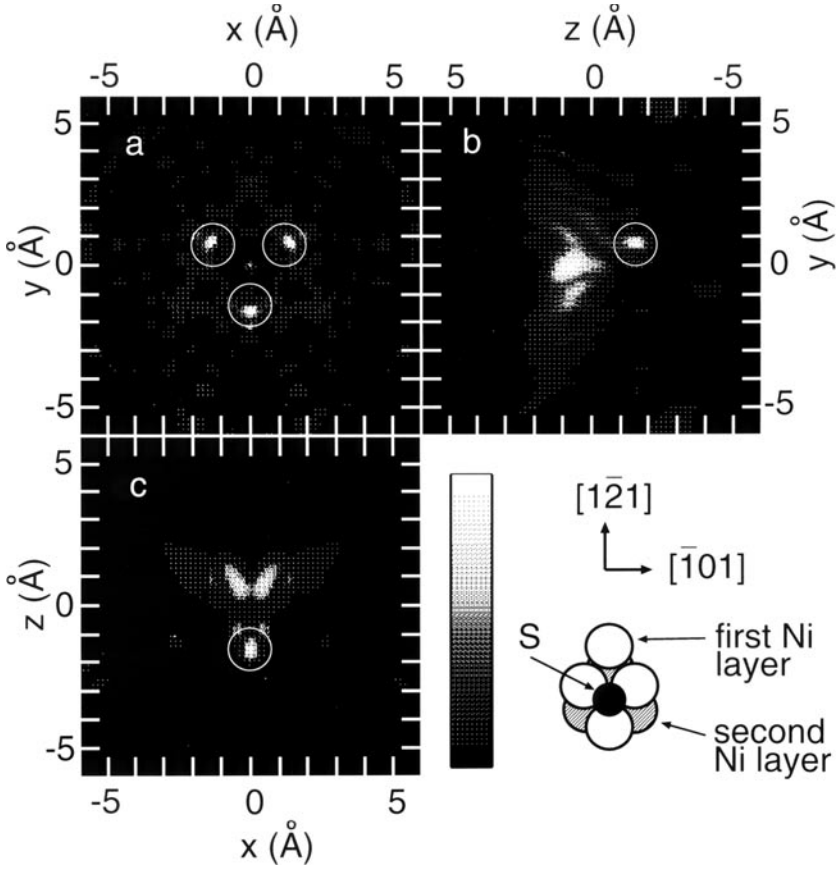

Figure 15. Holographic reconstruction obtained for the p(2 × 2)S/Ni(1 1 1) structure from seven different S $2p_{3/2}$ holograms, using the multiple wave number reconstruction approach (equation (6)). (a) represents a cut in the plane parallel to the Ni(1 1 1) surface at $z = -1.6$ Å (the surface of the substrate), (b) cut in a vertical plane parallel to the ($\underline{1}$0 1) plane at $x = 1.43$ Å, and (c) cut in a vertical plane parallel to the (1 $\underline{2}$ 1) plane at $y = 1.59$ Å. Note that cuts (b) and (c) are shifted from the 'correct' positions at $x = 1.25$ Å and $y = 1.44$ Å, respectively to pass through the atom images. The centres of the circles mark the expected positions of the Ni atoms for the case of a substrate–adsorbate distance of 1.6 Å and the fcc adsorption site. The shown directions and the schematic drawing of the crystallographic structure are related to a cut (a).

The artificial structure in the range $z > 0$ stems partly from the symmetry operations used to obtain the whole 2π hologram from the experimentally determined sector of 126°. This is concluded from the fact that this structure disappears when only the sector of measurements is used for reconstruction (figure 16). In this case, only the Ni atom that lies almost entirely inside the back-scattering sector (indicated by dashed lines in the schematic drawing at the bottom of figure 16) is observed, which is attributed to the maximum of the atomic scattering factor in the back-scattering direction (180°). The atomic image in figure 16 is broadened and anti-symmetrically shifted from the supposed position of the nickel atom compared to the corresponding image in figure 15; this is due to the limited range and asymmetry (with respect to the Ni atom under consideration) of the $\boldsymbol{k}$ space sector used for reconstruction.

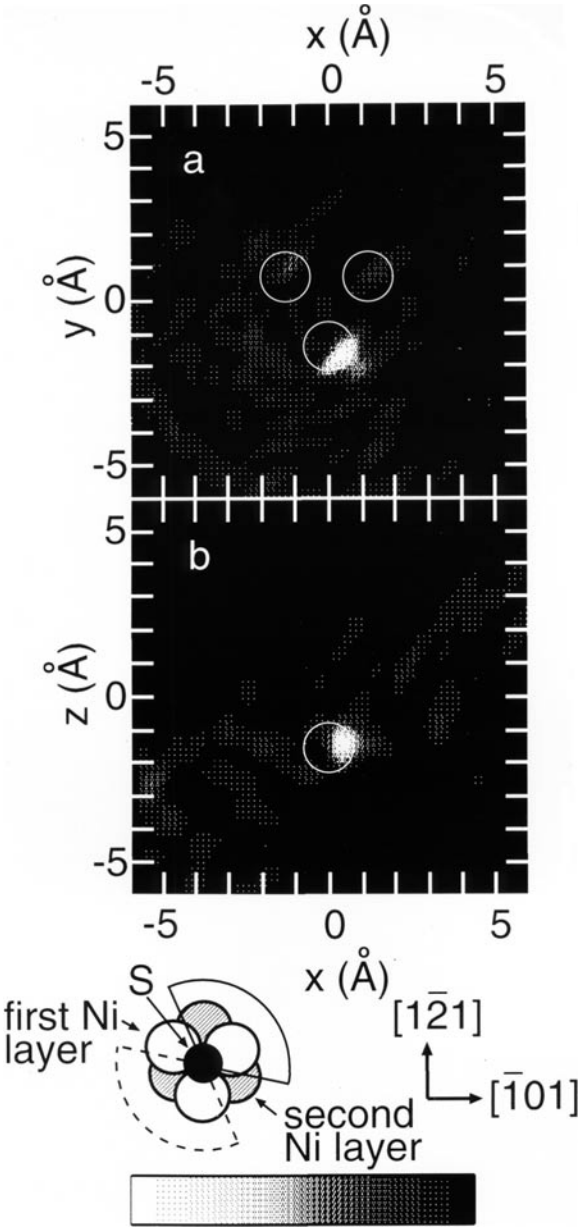

Figure 16. Holographic reconstruction obtained for the p(2 × 2)S/Ni(1 1 1) structure from seven different S $2p_{3/2}$ holograms, using the multiple wave number reconstruction approach (equation (6)). (a) represents a cut in the plane parallel to the Ni(1 1 1) surface at $z = -1.6$ Å (the surface of the substrate), (b) a cut in a vertical plane parallel to the (1 $\underline{2}$ 1) plane at $y = 1.59$ Å. Note that cut (b) is shifted from the 'correct' position at $y = 1.44$ Å to pass through the atom image. Only diffraction data within the sector of measurements (126°, shown in the schematic drawing below the cuts together with the backscattering sector by solid and dashed lines, respectively) were used. The centres of the circles mark the expected positions of the Ni atoms for the case of a substrate–adsorbate distance of 1.6 Å and the fcc adsorption site.

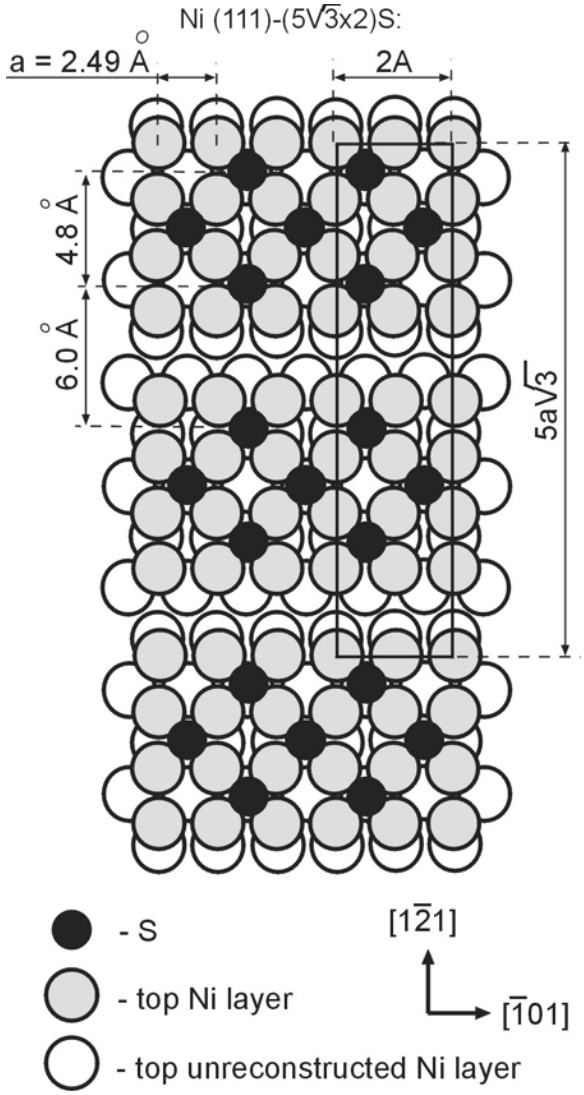

Figure 17. Model of the $(5\sqrt{3} \times 2)$ S/Ni(1 1 1) structure suggested in reference 43. The sulfur superstructure stems from the direct STM measurements [41].

3.2.3. Ni(1 1 1)-$(5\sqrt{3} \times 2)$ S. After showing that the adsorption site and adsorption geometry of S can be unequivocally identified using electron holography for the simple (2×2) structure, we wanted to test the potential of the method for a more complicated system, namely for the Ni(1 1 1)-$(5\sqrt{3} \times 2)$ S structure. For this structure different structural models have been proposed implying different reconstructions of the Ni(1 1 1) surface along with different S adsorption sites on the reconstructed (or non-reconstructed) surface [38–45]. The majority of the recent models suggest simple or pseudo-(1 0 0) reconstructions with shifted (see figure 17) or differently rotated four square-like tetramers of Ni atoms [43–45]. Sulfur is believed to occupy fourfold hollow sites on such a reconstructed surface with a distance to the topmost Ni layer of 0.8–1.2 Å.

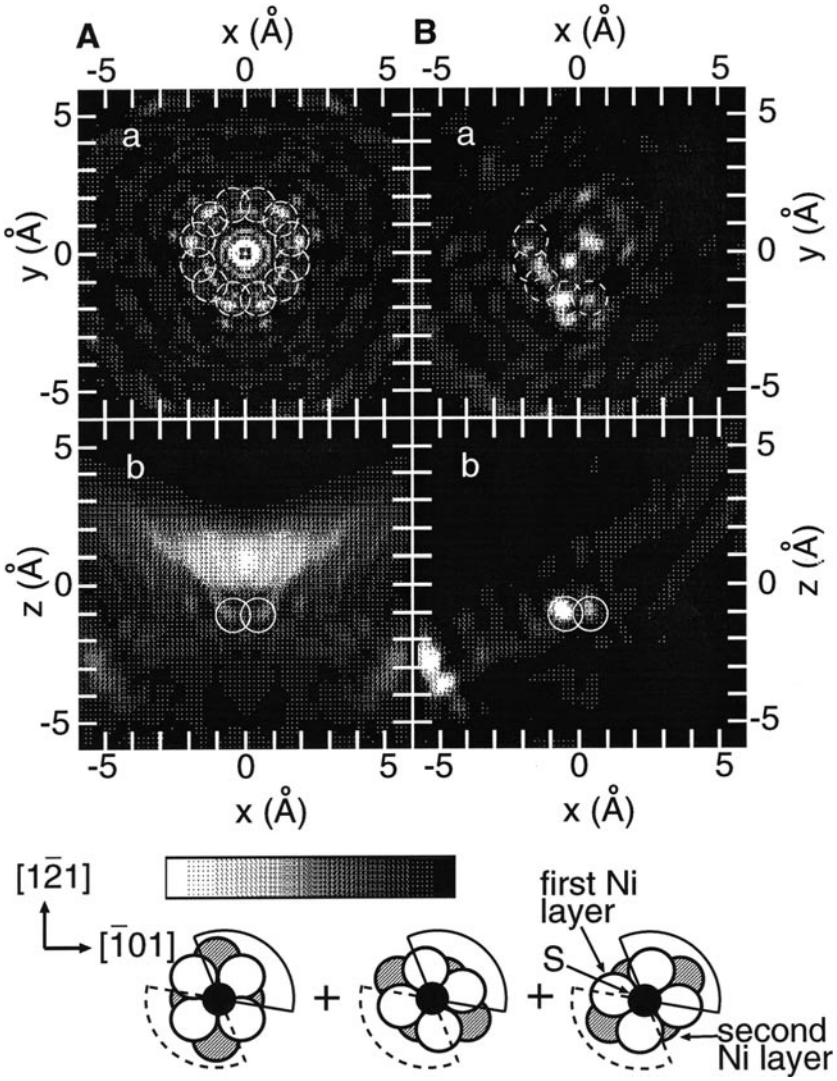

Figure 18. Holographic reconstruction for $(5\sqrt{3} \times 2)$S/Ni(1 1 1) from seven S $2p_{3/2}$ holograms at different energies using the multiple wave number approach (equation (6)). (a) represents a cut in a plane parallel to the Ni(1 1 1) surface at $z = -1.2$ Å and (b) a cut in a vertical plane parallel to the (1 $\underline{2}$ 1) plane at $y = -1.75$ Å. (A) has been obtained from the full hologram and (B) from the experimental sector only. The experimental sector of 126° is indicated by solid lines in the schematic drawing of the adsorption geometry for three different domains of the reconstructed Ni surface according to the model presented in figure 17. The backscattering sector is indicated by dashed lines. The centres of the circles mark the positions of the Ni atoms according to the structure suggested in reference 43 and shown in figure 17. The directions shown and the schematic drawing of the crystallographic structure are related to cuts (a).

As for Ni(1 1 1)-p(2 × 2) S, we have measured angular distributions of the S $2p_{3/2}$ photoelectrons ($E_B = 162$ eV) for seven different kinetic energies ranging from 130 eV ($k = 5.84$ Å^{-1}) to 322.5 eV ($k = 9.2$ Å^{-1}) for the Ni(111)-$(5\sqrt{3} \times 2)$ S system [19, 20] and processed all seven PED patterns within the multiple wave number reconstruction approach.

The holographic reconstructions of the Ni(111)-($5\sqrt{3} \times 2$) S system are completely different from those for the p(2×2) S structure. The most intense maxima in the physically meaningful region ($z < 0$) are now located at $z = -(1.0–1.2)$ Å. Reconstructed cuts in the $z = -1.2$ Å plane (a) along with cuts in the plane perpendicular to the surface along the [$\bar{1}$ 0 1] direction passing through some of the intense maxima in the $z = -1.2$ Å plane (b) are depicted in figure 18. The reconstruction in figure 18(A) has been obtained from the full 2π holograms and in figure 18(B), from the experimental sector of 126° only. The quality of the reconstructions is rather low (especially in figure 18(A); note that the abandonment of the symmetrization operation improves the quality of the reconstruction in the same way as for Ni(1 1 1)-p(2×2) S), which is attributed to the complexity of the ($5\sqrt{3} \times 2$) S structure and the superposition of the holographic contributions from different domains. Nevertheless, some qualitative and quantitative conclusions can be derived. First, the data are not consistent with the coexistence of many different adsorption sites (a small percentage of different adsorption sites, as suggested in references 44 and 45, can, however, not be excluded). Second, the relatively small distance of ∼1.2 Å to the top Ni layer rules out a threefold hollow adsorption site and indicates adsorption on a more open surface than an unreconstructed Ni(1 1 1).

The reconstructed image is approximately consistent with a quasi-(1 0 0) reconstruction of the Ni(1 1 1) crystal surface and a fourfold adsorption site of S on this surface [38, 43–45]. For comparison, the positions of the Ni atoms according to one of the models are depicted in figure 18 (circles) together with a schematic drawing of the adsorption geometry for three different domains of the reconstructed Ni surface [43].

4. Summary and conclusions

In conclusion, we have demonstrated with our work that the local geometrical structure of the clean single crystal surfaces and adsorbate systems can be successfully reconstructed using photoelectron holography with some restrictions. The main advantage of this method is that no preliminary assumptions about the structure of the investigated system are included in the reconstruction algorithm. We have consciously abandoned any correction for the anisotropy of the reference wave and the atomic scattering factor and used the holographic approach in its most direct form by going from the photoelectron holograms to the 3D reconstruction without any system-specific modifications of the reconstruction algorithm. Such an approach is best suited for characterizing unknown systems. Only Fourier filtering and multiplication by an apodizing function were applied; they turned out to be rather useful general tools for improving the quality of the holographic reconstruction.

Both forward- and back-scattering geometries were used. In agreement with the theoretical predictions, the choice of an appropriate reference wave (with a large angular momentum character) was found to be the decisive factor for the successful reconstruction of a surface structure in the forward-scattering geometry. We succeeded in reconstructing the structure of the Pt(1 1 0)-1×2 surface using a d/g photoelectron wave, but failed to reconstruct the structure of Ni(1 1 0) and Ni(1 1 1) (even by the multiple wave number approach) surfaces using a s/d photoelectron wave. For Ni(1 1 0) and Ni(1 1 1) only the atomic environment in the plane of the emitter parallel to the surface could be reconstructed due to the effective suppression of the most intense forward-scattering fringes (see the discussion in section 3.1.1). In the back-scattering geometry, the character of the reference wave seems to be of minor importance, but special care has to be taken of Debye–Waller losses.

The potential of both the single wave number and the multiple wave number phased sum approaches was tested. Single energy reconstructions were successful only in some cases; in general, they were found to strongly depend on the kinetic energy of the photoelectrons. This

can lead to an incorrect determination of the investigated structure in case of an unfortunate choice of kinetic energy. The use of PED patterns measured at different kinetic energies and the application of the multiple wave number phased sum method however, allow, avoidance of the problems related to the observed energy dependence of the single energy reconstructions. The results of this approach are not based on only one particular kinetic energy and are, therefore, more objective. Using this approach in the forward-scattering geometry we were able to reconstruct the structure of Ni(1 1 1) (only at $z = 0$) and Pt(1 1 0)-1 $\times$ 2. In back-scattering geometry we succeeded in determining the adsorption site of atomic S in the Ni(1 1 1)-p(2 $\times$ 2) S and Ni(111)-(5$\sqrt{3}$ $\times$ 2) S structures, in spite of the pronounced energy dependence of the single wave number reconstructions. Thus, the multiple wave number approach seems to be one method of choice in electron emission holography.

The reconstruction of the atomic arrangement within the adsorbate layer was not possible for the particular systems investigated because of the relatively large inter-adsorbate spacing and the small atomic number of sulfur. In principle, such a reconstruction should, however, be possible for adsorbates with a large atomic number. On the other hand, the holographic reconstruction of an adsorbate superstructure in the forward-scattering geometry seems to be altogether questionable because of the problem of non-equivalent emitters (see discussion in section 3.2.1).

The very large experimental dataset usually associated with photoelectron holography, especially with the multiple wave number approach (full-hemispherical PED patterns at various kinetic energies), can be reduced if diffraction data in a defined angular sector only (at best in the symmetry-irreducible one) are used for the reconstruction. This approach also leads to a reduction of artificial structures in both the forward- and back-scattering geometries as shown for Ni(1 1 1), Ni(1 1 1)-p(2 $\times$ 2) S and Ni(111)-(5$\sqrt{3}$ $\times$ 2) S. The idea of using a part of the hologram for the reconstruction was of importance for realizing that there are different ways to sample **k**-space within the electron emission holography (a similar approach was independently introduced by Thevuthasan *et al* [46]). As was shown by Len *et al* [47], the optimal **k**-space sampling should be intermediate between the extreme limits of scanned-angle or scanned-energy methods.

A more technical aspect is the usefulness of the Fourier filtering within the data processing procedure that was practically demonstrated in the present work following the original idea by Harp *et al* [4]. Later on, this tool was successfully used by other groups (see e.g. reference 48).

In summary, these results were a valuable contribution to the field. The experimental evidence for the importance of the suitable reference wave in the forward-scattering geometry is useful information for practical experimental work (an alternative way to suppress the forward-scattering effects was proposed by Greber and Osterwalder [49] and practically demonstrated by Wider *et al* [50]). Along with the theoretical and experimental results of other groups [16, 51, 52], the importance and applicability of the multiple wave number approach was experimentally demonstrated. The holographic reconstruction of Ni(1 1 1)-p(2 $\times$ 2) S performed within this approach was an important step in going from the model single crystal surfaces to adsorbate ensembles. Further development of electron emission holography [48, 53] and other direct methods for surface structure reconstruction such as projection method [54, 55], x-ray holography [56–63], and holographic LEED [64–72] unequivocally showed that the acquisition and joint processing of the diffraction data for multiple wave numbers are indispensable prerequisites for successful reconstruction.

As a concluding remark it is important to note that due to the limited spatial resolution of electron emission holography, it is not possible to determine the positions of adsorbates with very high accuracy; an approximate determination of the local structure around the

emitter can, however, be realized. The structural model can thereafter (if necessary) be refined by more accurate structural methods such as LEED and scanned energy PED which compare experimental datasets to calculations for various possible structures. Within such a combined approach, holographic reconstruction is an important step, which allows avoidance of ambiguity of the conventional 'trial and error' procedures and significant reduction in computational expenditures.

Acknowledgment

The major part of the work described in this review has been performed during the stay of the authors in the group of Prof Dr Dietrich Menzel (Physik Department E20) at the Technische Universität München. We would like to thank our collaborators on the project there, namely Dr Dietmar Mehl, Dr Martin Weinelt, Dr Peter Zebisch and Dr Markus Stichler (TU München) for the exciting time we spent together at the beamtimes at BESSY-I and in the lab in Munich trying to solve numerous experimental and computational problems. We are deeply indebted to Prof Dietrich Menzel for his support and for many valuable discussions. We also acknowledge P Averkamp and K Eberle for technical assistance and the BESSY-I staff, especially M Mast for technical help. M Z thanks the F V S Stiftung and the Hanns-Seidel-Stiftung for financial support. This work has been supported by the DFG (SFB 338) and the BMBF (05 5WO CAI).

References

[1] Szöke A 1986 Short Wavelength Coherent Radiation: Generation and Application *AIP Conf. Proc.* No 147 D TAttwood and J Boker (New York: AIP)
[2] Barton J J 1988 *Phys. Rev. Lett.* **61** 1356
[3] Barton J J 1990 *J. Electron Spectrosc. Relat. Phenom.* **51** 37
[4] Harp G R, Saldin D K, Chen X, Han Z L and Tonner B P 1991 *J. Electron Spectrosc. Relat. Phenom.* **57** 331
[5] Egelhoff Jr W F 1990 *Crit. Rev. Solid State Mat. Sci.* **16** 213
[6] Saldin D K, Harp G R, Chen B L and Tonner B P 1991 *Phys. Rev.* B **44** 2480
[7] Saldin D K, Harp G R and Tonner B P 1992 *Phys. Rev.* B **45** 9629
[8] Tonner B P, Han Z L, Harp G R and Saldin D K 1991 *Phys. Rev.* B **43** 14 423
[9] Tong S Y, Wei C M, Zhao T C, Huang H and Li Hua 1991 *Phys. Rev. Lett.* **66** 60
[10] Hardcastle S, Han Z L, Harp G R, Zhang J, Chen B L, Saldin D K and Tonner B P 1991 *Surf. Sci. Lett.* **245** L190
[11] Han Z L, Hardcastle S, Harp G R, Li H, Wang X D, Zhang J and Tonner B P 1991 *Surf. Sci.* **258** 313
[12] Tong S Y, Li Hua and Huang H 1991 *Phys. Rev. Lett.* **67** 3102
[13] Barton J J 1991 *Phys. Rev. Lett.* **67** 3106
[14] Huang H, Li Hua and Tong S Y 1991 *Phys. Rev.* B **44** 3240
[15] Li Hua, Tong S Y, Naumovic D, Stuck A and Osterwalder J 1993 *Phys. Rev.* B **47** 10 036
[16] Terminello L J, Barton J J and Lapiano-Smith D A 1993 *Phys. Rev. Lett.* **70** 59
[17] Zharnikov M, Mehl D, Weinelt M, Zebisch P and Steinrück H-P 1994 *Surf. Sci.* **306** 125
[18] Zharnikov M, Mehl D, Weinelt M, Zebisch P and Steinrück H-P 1994 *Surf. Sci.* **312** 82
[19] Zharnikov M, Weinelt M, Zebisch P and Steinrück H-P 1996 *Thin Solid Films* **275** 266
[20] Zharnikov M, Weinelt M, Zebisch P, Stichler M and Steinrück H-P 1995 *Surf. Sci.* **334** 114
[21] Zharnikov M, Weinelt M, Zebisch P, Stichler M and Steinrück H-P 1994 *Phys. Rev. Lett.* **73** 3548
[22] Huber W, Steinrück H-P, Pache T and Menzel D 1989 *Surf. Sci.* **217** 103
[23] Steinrück H-P, Huber W, Pache T and Menzel D 1989 *Surf. Sci.* **218** 293
[24] Bernstorff S, Braun W, Mast M, Peatman W and Schröder T 1989 *Rev. Sci. Instr.* **60** 2097
[25] Engelhardt H A, Bäck W, Menzel D and Liebl H 1981 *Rev. Sci. Instr.* **52** 835
Engelhardt H A, Zartner A and Menzel D 1981 *Rev. Sci. Instr.* **52** 1161
[26] Hoffmann P, Gossler J, Zartner A, Glanz M and Menzel D 1985 *Surf. Sci.* **161** 303
[27] Saiki R S, Kaduwela A P, Kim Y J, Friedman D J, Osterwalder J, Thevuthasan S and Fadley C S 1992 *Surf. Sci.* **279** 305
[28] Bao S, Schindler K M, Hofmann Ph, Fritzsche V, Bradshaw A M and Woodruff D P 1993 *Surf. Sci.* **291** 295

[29] Demuth J E, Marcus P M and Jepsen D W 1975 *Phys. Rev.* B **11** 1460
[30] Narusawa T, Gibson W M and Tornqvist E 1981 *Phys. Rev. Lett.* **47** 417
[31] Demuth J E, Jepsen D W and Marcus P M 1974 *Phys. Rev. Lett.* **32** 1182
[32] Baudoing R, Blanc E, Gaubert C, Gauthier Y and Gnuchev N 1983 *Surf. Sci.* **128** 22
[33] Baudoing R, Gauthier Y and Joly Y 1985 *J. Phys. C: Solid State Phys.* **18** 4061
[34] Capehart T W and Rhodin T N 1979 *J. Vacuum Sci. Technol.* **16** 594
[35] Warburton D R, Wincott P L, Thornton G, Quinn F M and Norman D 1989 *Surf. Sci.* **211–212** 71
[36] Fauster Th, Durr H and Hartwig D 1986 *Surf. Sci.* **178** 657
[37] Ku Yi Sha and Overbury S H 1992 *Surf. Sci.* **276** 62
[38] Edmonds T, McCarrol J J and Pitkethly R C 1971 *J. Vacuum Sci. Technol.* **8** 68
[39] Erley W and Wagner H 1978 *J. Catal.* **53** 287
[40] Delescluse P and Masson A 1980 *Surf. Sci.* **100** 423
[41] Ruan L, Stensgaard I, Besenbacher F and Laegsgaard E 1993 *Phys. Rev. Lett.* **71** 2963
[42] Ruan L, Stensgaard I, Besenbacher F and Laegsgaard E 1994 *Phys. Rev. Lett.* **72** 2500
[43] Gardin D E, Batteas J D, Van Hove M A and Somorjai G A 1993 *Surf. Sci.* **296** 25
[44] Foss M, Feidenhans'l R, Nielsen M, Findeisen E, Johnson R L, Buslaps T, Stensgaard I and Besenbacher F 1994 *Phys. Rev.* B **50** 8950
[45] Lüdecke J, Ettema A H H F, Driver S M, Scragg G, Kerkar M, Woodruff D P, Cowie B C C, Jones R G and Bastow S 1996 *Surf. Sci.* **366** 260
[46] Thevuthasan S, Ynzunza R X, Tober E D, Fadley C S, Kaduwela A P and Van Hove M A 1993 *Phys. Rev. Lett.* **70** 595
[47] Len P M, Thevuthasan S, Kaduwela A P, Van Hove M A and Fadley C S 1996 *Surf. Sci.* **365** 535
[48] Terminello L J, Peterson B L and Barton J J 1995 *J. Electron Spectrosc. Relat. Phenom.* **75** 299
[49] Greber T and Osterwalder J 1996 *Chem. Phys. Lett.* **256** 653
[50] Wider J, Baumberger F, Sambi M, Gotter R, Verdini A, Bruno F, Cvetko D, Morgante A, Freber T and Osterwalder J 2001 *Phys. Rev. Lett.* **86** 2337
[51] Tong S Y, Huang H and Wei C M 1992 *Phys. Rev.* B **46** 2452
[52] Tobin J G, Waddill G D, Li H and Tong S Y 1993 *Phys. Rev. Lett.* **70** 4150
[53] Banerjee S, Ravy S, Denlinger J, Chen X, Saldin D K and Tonner B P in preparation
[54] Hofmann Ph and Schindler K-M 1993 *Phys. Rev.* B **47** 13 941
[55] Hofmann Ph, Schindler K-M, Bao S, Bradshaw A M and Woodruff D P 1994 *Nature* **368** 131
[56] Tegze M and Faigel G 1996 *Nature* **380** 49
[57] Gog T, Len P M, Materlik G, Bahr D, Fadley C S and Sanchez-Hanke C 1996 *Phys. Rev. Lett.* **76** 3132
[58] Gog T, Menk R-H, Arfelli F, Len P M, Fadley C S and Materlik G 1996 *Synchr. Radiat. News* **9** 30
[59] Hayashi K, Yamamoto T, Kawai J, Suzuki M, Goto S, Hayakawa S, Sakurai K and Gohshi Y 1998 *Anal. Sci.* **14** 987
[60] Hiort T, Novikov D V, Kossel E and Materlik G 2000 *Phys. Rev.* B **61** R830
[61] Tegze M, Faigel G, Marchesini S, Belakhovsky M and Ulrich O 2000 *Nature* **407** 38
[62] Korecki P, Materlik G and Korecki J 2001 *Phys. Rev. Lett.* **86** 1534
[63] Korecki P and Materlik G 2001 *Phys. Rev. Lett.* **86** 2333
[64] Wei C-M, Tong S Y, Wedler H, Mendez M A and Heinz K 1994 *Phys. Rev. Lett.* **72** 2434
[65] Saldin D K and Chen X 1995 *Phys. Rev.* B **52** 2941
[66] Saldin D K, Reuter K, De Andres P L, Wedler H, Chen X, Pendry J B and Heinz K 1996 *Phys. Rev.* B **54** 8172
[67] Reuter K, Bernhardt J, Wedler H, Schardt J, Starke U and Heinz K 1997 *Phys. Rev. Lett.* **79** 4818
[68] Reuter K, Wedler H, Ott M, Heinz K, Vamvakas J A, Chen X and Saldin D K 1997 *Phys. Rev.* B **55** 5344
[69] Saldin D K, Chen X, Vamvakas J, Ott M, Wedler H, Reuter K, Heinz K and De Andres P L 1997 *Surf. Rev. Lett.* **4** 991
[70] Reuter K, Vamvakas J A, Saldin D K, Blum V, Ott M, Wedler H, Döll R and Heinz K 1998 *Phys. Rev.* B **58** 4102
[71] Seubert A, Saldin D K, Bernhardt J, Starke U and Heinz K 2000 *J. Phys.: Condens. Matter* **12** 5527
[72] Heinz K, Starke U and Bernhardt J 2000 *Progr. Surf. Sci.* **64** 163